Proton and Electron Transfer to the Secondary Quinone (Q_B) in Bacterial Reaction Centers: The Effect of Changing the Electrostatics in the Vicinity of Q_B by Interchanging Asp and Glu at the L212 and L213 Sites[†]

M. L. Paddock, G. Feher, and M. Y. Okamura*

Department of Physics, 0319, University of California, San Diego, 9500 Gilman Drive, La Jolla, California 92093-0319

Received May 21, 1997; Revised Manuscript Received August 28, 1997[⊗]

ABSTRACT: The bacterial reaction center (RC) plays a central role in photosynthetic energy conversion by facilitating the light induced double reduction and protonation of a bound quinone molecule, Q_B. Two carboxylic acid residues, Asp-L213 and Glu-L212, located near Q_B, were previously shown to be important for proton transfer to Q_B. In this work, the ability of Glu to substitute for Asp at L213 and Asp to substitute for Glu at L212 was tested by site-directed mutagenesis. Both single mutants and a double mutant in which Asp and Glu were exchanged between the two sites were constructed. The electron transfer rate constants k_{BD} ($D^+Q_AQ_B^- \rightarrow DQ_AQ_B$), and $k_{AB}^{(2)}$ ($DQ_A^-Q_B^- + H^+ \rightarrow DQ_A(Q_BH)^-$), that are known to be sensitive to the energy of the Q_B^- state, were found to be altered by Asp/Glu substitutions. Both rates were fastest (∼10-fold) in RCs with Asp at both sites, slowest with Glu at both sites (∼50-fold) and relatively unchanged by the caboxylic acid exchange. These changes could be explained if Asp was predominantly ionized and Glu was predominantly protonated at both sites (pH 7.5). The charge recombination k_{BD} suggests an observed ∼5 pK_a unit difference of Glu over Asp. Modeling of k_{BD} by strong electrostatic interactions (∼3−4 pK_a units) among negatively charged acids and Q_B^- indicated a lower intrinsic pK_a for Asp compared to Glu at either site of ∼2−3 units. The mechanism of the $k_{AB}^{(2)}$ reaction was determined to be the same in all mutant RCs as for native RCs. A quantitative explanation of the effect of the electrostatic environment on $k_{AB}^{(2)}$ was obtained using the two-step model proposed for native RCs [Graige, M. S., Paddock, M. L., Bruce, J. M., Feher, G., & Okamura, M. Y. (1996) *J. Am. Chem. Soc. 118*, 9005−9016] which involves fast protonation of the semiquinone followed by rate-limiting electron transfer. Using simple models for the quinone/quinol conversion rate, it is shown that the optimal electrostatic potential for the Q_B site is close to that found in native RCs.

The photosynthetic bacterial reaction center (RC)[1] is a membrane-bound pigment protein complex that performs the primary photochemistry by coupling light-induced electron transfer to vectorial proton transfer across the bacterial membrane. The isolated bacterial RC is composed of three polypeptide subunits (L, M, and H); four bacteriochlorophylls; two bacteriopheophytins; one non-heme Fe^{2+}; and two ubiquinone (UQ_{10}) molecules (reviewed in refs 1 and 2). In the RC, light-induced electron transfer proceeds from a primary donor (a bacteriochlorophyll dimer) through a series of electron donor and acceptor molecules (a bacteriopheophytin and a quinone molecule Q_A) to a loosely bound secondary quinone Q_B, which serves as a mobile electron and proton carrier (*3*−*5*). The reduction of Q_B to dihydroquinone Q_BH_2 involves the transfer of two electrons and two protons. The effect of replacing several carboxylic acid residues of the L subunit that change the electrostatic potential near Q_B is the subject of this investigation.

The first electron transfer to Q_B does not involve direct protonation of the quinone molecule; however, nearby amino acid residues change their protonation state in response to the change in the electrostatic field associated with the formation of Q_B^- (*6*, *7*). The second electron transfer ($k_{AB}^{(2)}$) is coupled with direct protonation of the quinone as shown in reactions 1a and 1b.

$$Q_A^-Q_B^- + H^+ \rightarrow Q_AQ_BH^- \quad (1a)$$

$$Q_AQ_BH^- + H^+ \rightarrow Q_AQ_BH_2 \quad (1b)$$

After reduction to Q_BH_2, the dihydroquinone dissociates from the RC (*8*) and releases its protons on the periplasmic side of the membrane, resulting in the formation of a proton gradient that drives ATP synthesis (reviewed in refs 9 and 10). The vacant Q_B site of the RC becomes occupied by a free quinone molecule from the membrane pool, resetting the photocycle for an additional turnover (Figure 1).

The Q_B binding site of the bacterial RC is in the interior of the protein out of direct contact with the solvent (*11*−*24*). It has been established that specific amino acid residues of the L subunit are important for proton transfers necessary for the formation of the dihydroquinone. On the basis of investigations of the kinetics of electron transfer and proton uptake from solution in native and site-directed mutant RCs, a separate proton transfer pathway has been proposed for

[†] Work supported by National Science Foundation (NSF MCB94-16652 and 96-30215) and National Institutes of Health (NIH GM 41637 and NIH GM 13191).

* To whom correspondence should be addressed.

[⊗] Abstract published in *Advance ACS Abstracts,* November 1, 1997.

[1] Abbreviations: D, primary donor; Q_A, primary quinone acceptor; Q_B, secondary quinone acceptor; Q, quinone molecule; QH_2, dihydroquinone; UQ_{10}, ubiquinone-10 (2,3-dimethoxy-5-methyl-6-decaisoprenyl-1,4-benzoquinone); MQ_4, menaquinone-4 (2-methyl-3-tetraisoprenyl-1,4-naphthoquinone); TEMNQ, tetramethylnaphthoquinone (2,3,6,7-tetramethyl-1,4-naphthoquinone); RC, reaction center; cyt *c*, horse heart cytochrome *c*; bp, base pair; HME, 10 mM Hepes, pH 7.5, 0.04% maltoside, 0.1 mM EDTA.

S0006-2960(97)01192-6 CCC: $14.00 © 1997 American Chemical Society

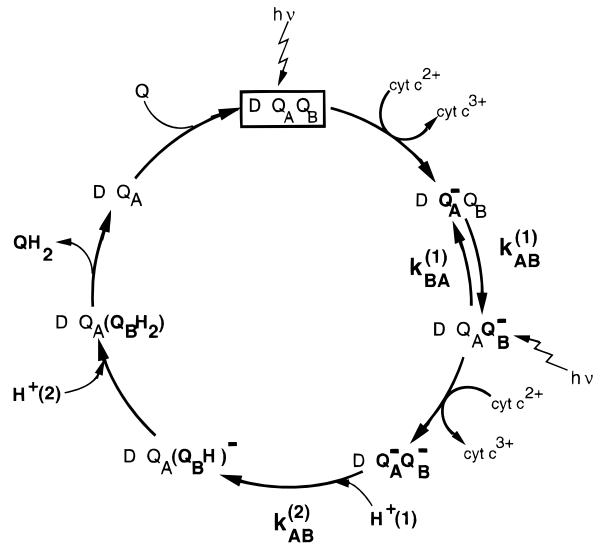

FIGURE 1: Photochemical cycle of reaction centers showing electron transfer, proton uptake, quinone exchange and cytochrome oxidation. The first and second electron transfer rate constants are indicated as $k_{AB}^{(1)}$ and $k_{AB}^{(2)}$, respectively. The transfer of the second electron to Q_B involves the uptake of the first proton $H^+(1)$. The transfer of a second proton $H^+(2)$ to reduced Q_B is not a prerequisite for the second electron transfer (see text). The cycling rate for native RCs is $\sim 10^3$ s^{-1}.

each reaction, 1a and 1b. The proton pathway for reaction 1b involves Glu-L212, which is in the vicinity of Q_B (*25*, *26*). Replacement of Glu-L212 with Gln resulted in relatively little change in the measured electron transfer rates of the first and second electron (*25*, *26*) but in a significantly slower proton uptake following the two electron reduction of Q_B (reaction 1b) (*27*, *28*). This was attributed to a blockage of proton transfer to reduced Q_B in the mutant RCs. This replacement did not affect the electrostatic environment near Q_B as shown by the similar value of the recombination rate constant k_{BD} ($D^+Q_AQ_B^- \rightarrow DQ_AQ_B$) to that seen in native RCs. This suggests that *Glu-L212 in native RCs is predominantly protonated (neutral)* (*25*, *26*).

The proton transfer pathway for reaction 1a involves Ser-L223 and Asp-L213, both located in the vicinity of Q_B, most likely as components of a proton transfer chain (*26*, *28*−*35*). Replacement of Asp-L213 with Asn resulted in a smaller value for $k_{AB}^{(2)}$, presumably a consequence of removing a component of a proton transfer chain, and a smaller value for k_{BD}. This suggests that *Asp-L213 in native RCs is predominantly ionized*, which accelerates the recombination reaction. It has also been suggested that Asp-L213 is important for establishing a negative potential near Q_B to favor its protonation. This suggestion is based on the observation that substitution of Asp-L213 by Glu changes both k_{BD} and $k_{AB}^{(2)}$ (*35*). Site-directed mutations constructed at other sites near Q_B (*36*−*41*) analogously produce electrostatic and functional changes. Electrostatic calculations by Beroza *et al.* (*42*, *43*), Gunner and Honig (*44*), and Lancaster *et al.* (*45*) have shown that such interactions within the RC protein can be very large and have a significant influence on the behavior of internal carboxylic acids. Another line of research that supports the proposal that electrostatics are important for RC function, *e.g.* efficient proton transfer, comes from work on spontaneous photosynthetic revertants of detrimental site-directed replacements (*46*−*50*). In all cases a compensating (suppressor) mutation to the detrimental Asp-L213 → Asn (or Ala) mutation involved a change in charge, from positive to neutral or neutral to negative, at the suppressor site; this conclusion is supported by altered charge recombination kinetics which probes the elecrostatic environment (*47*, *50*).

In this paper, we test the effect of the electrostatic environment near Q_B on the function of the RC. The electrostatics were changed by substituting Asp for Glu at the L212 site and Glu for Asp at the L213 site. Single mutations of Asp-L213 → Glu and Glu-L212 → Asp and the double mutant Glu-L212 → Asp/Asp-L213 → Glu were constructed in RCs from *Rhodobacter (Rb.) sphaeroides*. Bacteria harboring these mutations were tested for photosynthetic viablity. Isolated RCs were characterized with respect to their proton-coupled electron transfer rate constant $k_{AB}^{(2)}$ (reaction 1a), and the first electron transfer rate constant $k_{AB}^{(1)}$ ($Q_A^-Q_B \rightarrow Q_AQ_B^-$) charge recombination rate constant k_{BD} ($D^+Q_AQ_B^- \rightarrow DQ_AQ_B$), which is sensitive to the charged state of the amino acid residue (*i.e.* electrostatic potential) near Q_B. The titration of the amino acid residues near Q_B was investigated by determining the pH dependences of the rate constants. The results are discussed in light of interacting titrating residues and the proposed mechanism of proton-coupled electron transfer associated with reaction 1a for native RCs (*51*, *52*). The importance of the elecrostatic environment near Q_B for photosynthetic function is discussed. A preliminary account of this work has been presented (*53*).

MATERIALS AND METHODS

Materials

Dodecyl β-D-maltoside was obtained from Calbiochem or Anatrace and *N*,*N*-dimethyldodecylamine *N*-oxide (LDAO) from Fluka Chemie. Ubiquinone-50 obtained from Sigma was solubilized at 50 °C in either 10% deoxycholic acid (at ~1 mM quinone) or 1% LDAO (at ~0.2 mM quinone) and stored at −70 °C. The inhibitors terbutryne, 1,10-phenanthroline, and stigmatellin were from Chem Services, Fisher Scientific, and Fluka, respectively. Restriction enzymes and other DNA modifying enzymes used in the site-directed mutagenesis procedures were obtained as described by Paddock *et al.* (1989). The site-directed mutagenesis kit was obtained from Amersham. The BBL GasPak 100 and 150 Jar Systems were obtained from Fisher Scientific. All other chemicals were of reagent or HPLC grade.

Site-Directed Mutagenesis

The construction of the Asp-L213 → Glu [DE(L213)] was previously described by Paddock *et al.* (*35*). The Glu-L212 → Asp [ED(L212)] was constructed as previously described by Paddock *et al.* (*25*) using the Amersham oligonucleotide-directed mutagenesis kit based upon the method developed by Nakamaye and Eckstein (*54*) and the oligonucleotide 5′-CGGATCAC **GAC** GATACGTT-3′ carrying the **GAC** codon changes for the Glu-L212 → Asp replacement. The double mutant ED(L212)/DE(L213) was constructed as described (*35)* using the oligonucleotide 5′-CCGGATCAC **GAC GAG** ACGTTCTTCCGC-3′ carrying the **GAC** and **GAG** codon changes for the Glu-L212 → Asp and Asp-L213 → Glu replacements.

The mutations were incorporated into an M13 vehicle containing the *Asp* 718−*Hin*dIII fragment of *pufL* (*55*) which codes for the latter two-thirds of the L subunit. Mutants were identified by single lane sequencing of phage DNA

from several plaques. A uniform phage culture for each replacement was obtained by reinfection into *Escherichia coli* followed by isolation of an individual plaque. Only the desired changes were found by DNA sequence in the *Asp* 718−*Hin*dIII region. This fragment was then exchanged with the kanamycin fragment of pRKSCHKm (*55*), transformed into *E. coli* S17−1 (*56*), and mated into the *Rb. sphaeroides* deletion strain ΔLM1 (*25*), resulting in the complemented deletion strains. These strains were grown semiaerobically to induce RC production without applying selection for photosynthetic growth as described by Paddock *et al.* (*25*).

Photosynthetic Growth

The complemented deletion strains carrying the native or site-directed modified RC genes were tested for their ability to grow under anaerobic photosynthetic conditions as previously described by Rongey *et al.* (*57*). Briefly, the deletion strain complemented with native or mutant genes was restricted to anaerobic photosynthetic conditions using the BBL Gas Pak 100 or 150 Jar Systems at 32 °C. Control plates with a comparable number of bacteria were grown aerobically to determine the original viable cell density. Between $\sim 10^5$ and $\sim 10^7$ viable bacteria were spread evenly onto each plate before subjecting the RCs to either aerobic or anaerobic photosynthetic conditions. The number of colonies present on the plate restricted to anaerobic photosynthetic conditions was compared after 5−7 days to the number of colonies present on the plate grown under aerobic nonselective conditions to determine photosynthetic viability of the strains carrying site-directed mutations in the RC.

Reaction Center Preparation

RCs were isolated from *Rb. sphaeroides* R26 (native) or from the mutants (*Rb. sphaeroides* 2.4.1-based mutations) in LDAO as described (*58*); they contained approximately 1−1.5 ubiquinone molecules per RC as determined by standard methods (*59*) and had an observed ratio of $A_{280}^{1cm}/A_{802}^{1cm} \leq 1.3$. The RC concentration was determined (*27*) by the amount of cyt *c* oxidized (measured at 550 nm) after one saturating laser flash using the extinction coefficients $\Delta\epsilon_{550}(\text{cyt } c^{2+} - \text{cyt } c^{3+}) = 21.1\ \text{mM}^{-1}\ \text{cm}^{-1}$ (*60*). Reconstitution of UQ into the Q_B site of the RCs was accomplished as follows: a 5−10-fold excess of UQ_{10} was added to the RC solution which was then dialyzed for 2 days against 10 mM Hepes, pH 7.5, 0.04% dodecyl β-D-maltoside, 0.1 mM EDTA. Incorporation of menaquinone-4 (MQ_4) and tetramethylnaphthoquinone (TEMNQ) was accomplished as described by Graige *et al.* (*52*) as modified below: RCs with approximately one quinone per RC were added to a glass vial in which an ethanolic solution of MQ_4 or TEMNQ was previously dried. The solution was incubated at 30 °C for approximately 1 h to allow the solution to saturate with either MQ_4 or TEMNQ and to establish an equilibration between UQ_{10} and the naphthoquinone for binding to the Q_A site of the RCs. Usually the Q_A site contained 25−50% MQ_4 or TEMNQ and the Q_B site was occupied to >60% with UQ_{10}; neither MQ_4 nor TEMNQ binds competitively to the Q_B site.

Electron Transfer Rate Measurements

The kinetics of electron transfer were determined from absorption changes recorded on a modified Cary 14 spectrophotometer (Varian) as described by Kleinfeld *et al.* (*59*). Voltage output from the amplifier was recorded on a digital oscilloscope (LeCroy 9310M) and transferred to a personal computer (PC) for storage and analysis. Kinetic data traces were fitted to exponential functions on a PC using nonlinear curve fitting software (Peakfit or Sigmaplot, Jandel). Actinic illumination was provided by a pulsed dye laser (Phase R DL2100c; 590 nm, ∼0.2 J/pulse, 0.5 μs pulse width). All measurements were performed with 1−3 μM RCs in 10 mM buffer(s), 0.04% dodecyl β-D-maltoside, and 0.1 mM EDTA at 23 °C.

The rate constant for the transfer of the first electron to Q_B, $k_{AB}^{(1)}$, was measured by monitoring the bacteriopheophytin band shift at 750 nm, which is sensitive to the reduction state of the quinones Q_A and Q_B (*59*, *61*). To obtain better signal-to-noise ratios, 9 to 36 traces were averaged from the same sample on the LeCroy oscilloscope prior to transfer to the PC.

The measured rate constant for the double reduction of Q_B, $k_{AB}^{(2)}$ (reaction 1a), was determined by measuring the decay after a second laser flash of the semiquinone absorption at 450 nm (*62*) in the presence of 20−50 μM cytochrome *c* (cyt *c*) or 20−200 μM ferrocene, which reduces the donor after each flash. In RCs with MQ_4 added to occupy the Q_A site (see above), biphasic kinetics were observed at 450 nm with one rate corresponding to the rate observed in RCs with UQ_{10} occupying the Q_A site ($k_{AB}^{(2)} \sim 1500\ s^{-1}$, pH 7.5, native RCs) and the other rate attributed to RCs with MQ_4 occupying the Q_A site ($k_{AB}^{(2)} \sim 6000\ s^{-1}$, pH 7.5, native RCs). The relative occupancies of UQ_{10} and MQ_4 determined by this manner agreed with the relative occupancies determined from the deconvolution of biphasic kinetics for k_{AD} (see below).

The charge recombination rate $D^+Q_A^- \rightarrow DQ_A$ (k_{AD}) was determined from the rate of recovery of the oxidized donor monitored at 865 nm following a saturating laser flash in RCs containing only Q_A. In the samples to which naphthoquinone was added, the relative occupancies of the two quinones in the Q_A site could be determined from a deconvolution of the charge recombination kinetics, since k_{AD} is faster (50−100%) in RCs with a naphthoquinone in the Q_A site than with UQ_{10} in the Q_A site.

The charge recombination rate $D^+Q_AQ_B^- \rightarrow DQ_AQ_B$ (k_{BD}) was determined from the kinetics of the slow phase of the donor recovery (>60% of the amplitude) in RC samples in the presence of excess UQ_{10}. The pH of the solution was adjusted by adding acid (1 N HCl) or base (1 N NaOH) to a mixture of buffers containing Caps, Ches, Mes, Pipes, and Tris at 2.5 mM each.

Determination of the Free Energy of the $Q_AQ_B^-$ State with Respect to the $Q_A^-Q_B$ State

The equilibrium energy between the states $Q_AQ_B^-$ and $Q_A^-Q_B$ can be obtained from the measured charge recombination rate constants k_{AD} and k_{BD}. In principle, the mechanism of charge recombination $D^+Q_AQ_B^- \rightarrow DQ_AQ_B$ has contributions both from indirect recombination *via* thermal population of the $D^+Q_A^-Q_B$ state, k_{BD}^{ind} (see eq 2), and from direct recombination back to the ground state, k_{BD}^{dir}:

$$k_{BD} = k_{BD}^{ind} + k_{BD}^{dir} \quad (2)$$

The indirect mechanism was shown to be dominant for charge recombination in native RCs (*59*) and is sensitive to the energy gap between the $Q_AQ_B^-$ and $Q_A^-Q_B$ states. In this case, the indirect charge recombination rate constant k_{BD}^{ind} is related to k_{AD} and the fraction of RCs in the $D^+Q_A^-Q_B$ state, α (*59*), *i.e.*

$$k_{BD}^{ind} = k_{BD} - k_{BD}^{dir} = \alpha k_{AD} \quad (3)$$

The equilibrium constant K between the $D^+Q_AQ_B^-$ and $D^+Q_A^-Q_B$ states is given by

$$K = \frac{[D^+Q_AQ_B^-]}{[D^+Q_A^-Q_B]} = \frac{1-\alpha}{\alpha} = \exp(-\Delta G^0/kT) \quad (4)$$

where k is Boltzmann's constant, and T is the absolute temperature, and ΔG^0 is the free energy difference between the $Q_AQ_B^-$ and $Q_A^-Q_B$ states. Combining eqs 3 and 4 we obtain

$$\Delta G^0 = -kT \ln\left(\frac{1-\alpha}{\alpha}\right) = -kT \ln\left(\frac{k_{AD} - k_{BD}^{ind}}{k_{BD}^{ind}}\right) \quad (5)$$

Assuming that the mechanism of charge recombination remains the same in the mutant RCs, the free energy difference ΔG^0 in the mutant RCs can be obtained from the determined values of k_{BD}^{ind} and k_{AD}. The forward rate constant $k_{AB}^{(1)}$ can be obtained from the observed $k_{AB}^{(1)obs}$ (as measured at 750 nm) using the relation

$$k_{AB}^{(1)} = k_{AB}^{(1)obs}\left(\frac{K}{1+K}\right) \quad (6)$$

RESULTS AND ANALYSIS

Photosynthetic Growth

The mutants, *i.e.* complemented deletion strains carrying the replacements in *pufL* (the L subunit gene), were tested for their ability to grow under anaerobic photosynthetic conditions. The number of colonies present on a plate grown under photosynthetic conditions was compared to an identical plate grown under nonselective aerobic conditions. The total number of bacteria used was between $\sim 10^5$ and $\sim 10^7$ spread onto each plate. The complemented deletion strain carrying the native *puf* operon, which includes the genes coding for the native L and M subunits, showed a comparable number of colonies on duplicate plates grown under aerobic and anaerobic (photosynthetic) conditions. The complemented deletion strains carrying the ED(L212) or ED(L212)/DE-(L213) mutations also showed a similar number of viable colonies when grown under either aerobic or anaerobic conditions (data not shown). In contrast, the complemented deletion strains carrying the DE(L213) mutation showed only a small fraction ($<10^{-5}$) of colonies on the anaerobic plate compared to the aerobic plate. The small number of photosynthetic colonies is attributed to spontaneous photosynthetic revertants containing suppressor mutations that restore photosynthetic function to the RCs. Thus, the ED-(L212) and ED(L212)/DE(L213) were observed to be photosynthetically competent while the DE(L213) was not.

Charge Recombination Rates

The charge recombination rates contain important information about the electrostatic environment in the vicinity of the reduced quinone. The charge recombination rates $D^+Q_A^- \rightarrow DQ_A$ (k_{AD}) and $D^+Q_AQ_B^- \rightarrow DQ_AQ_B$ (k_{BD}) were measured by monitoring the change in absorption of the primary electron donor at 865 nm (Table 1).

Table 1: Amino Acid Residues, Kinetic Rate Constants, Equilibrium Constant K, and Free Energy Differences $\delta\Delta G^0$ (pH 7.5, T = 23 °C) for Native and Mutant RCs[a]

strain	L212	L213	k_{AD}	k_{BD}	$k_{AB}^{(1)}$ [b]	$k_{AB}^{(2)}$	K[c]	$\delta\Delta G^0$ [d]
ED(L212)	Asp	Asp	10	8	300	8000	0.2	+100
native	**Glu**	**Asp**	**9**	**0.7**	**6300**	**1200**	**12**	**0**
ED(L212)/DE(L213)	Asp	Glu	9	0.7	5500	130	12	0
DE(L213)	Glu	Glu	9	0.02[e]	5000	18	1200	−110

[a] The RCs are arranged from the largest to smallest value for $k_{AB}^{(2)}$. Errors in the rates are estimated to be ∼10% for the charge recombination rate constants k_{AD} and k_{BD} and ∼25% for the forward electron transfer rate constants $k_{AB}^{(1)}$ and $k_{AB}^{(2)}$. The estimated errors are larger for the ED(L212) RCs due to a smaller fraction of Q_B^- formation (∼20% for k_{BD} and ∼35% for $k_{AB}^{(1)}$ and $k_{AB}^{(2)}$). [b] This is the forward electron transfer rate (Figure 1). This value was obtained from the observed rate and the equilibrium constant K using eq 6. [c] Calculated using the data in this table and eq 4. [d] Defined as ΔG^0(mutant) − ΔG^0(native); ΔG^0 values obtained from eq 5. [e] Since the rate of charge recombination was not affected by the substitution of lower potential quinones into the Q_A site, the charge recombination occurs predominantly directly from $D^+Q_AQ_B^-$ to DQ_AQ_B without involvement of the $D^+Q_A^-Q_B$ state (*73*).

Charge Recombination k_{AD}: $D^+Q_A^- \rightarrow DQ_A$. The recombination rate constant, k_{AD}, was measured in RCs containing only one ubiquinone (Q_A) and was found to be essentially the same in native and in all of the mutant RCs (k_{AD} = 10 ± 1 s^{-1}). RCs containing a naphthoquinone in the Q_A site showed faster recombination rates (∼20 s^{-1} for MQ_4 and ∼40 s^{-1} for TEMNQ) for native and mutant RCs consistent with a change in the redox potential of Q_A^-/Q_A upon quinone replacement.

Charge Recombination k_{BD}: $D^+Q_AQ_B^- \rightarrow DQ_AQ_B$. The recombination rate constant, k_{BD}, was measured in the presence of excess UQ_{10} [5−10 UQ_{10}/RC]. It was determined from the kinetics of the slow phase of charge recombination at 865 nm. The slow phase was absent in the presence of 1 mM 1,10-phenanthroline or 10 μM stigmatellin showing that this phase depends on the presence of Q_B and is attributed to the reaction $D^+Q_AQ_B^- \rightarrow DQ_AQ_B$.

The k_{BD} value measured for DE(L213) RCs (pH 7.5) was significantly smaller than the value for native RCs (Table 1), suggesting that the $Q_AQ_B^-$ state is lower in energy in the DE(L213) RCs compared to native RCs. In addition, k_{BD} was independent of the nature of the quinone occupying the Q_A site (*i.e.* independent of the $Q_A^-Q_B$ energy level) indicating that the observed recombination rate occurs predominantly through the direct pathway in this mutant RC. The ED(L212) RCs displayed significantly faster kinetics suggesting that Q_B^- is less stable in these mutant RCs. RCs from the double mutant ED(L212)/DE(L213) displayed k_{BD} values comparable to native RCs (Table 1). The recombination for native, ED(L212), and ED(L212)/DE(L213) RCs was dominated by the indirect pathway as shown by the significant decrease in k_{BD} (∼5-fold) in RCs containing a naphthoquinone in the Q_A site (see *e.g.* ref 63).

The pH dependences of k_{BD} for native and mutant RCs are shown in Figure 2. Native RCs show two pH dependent

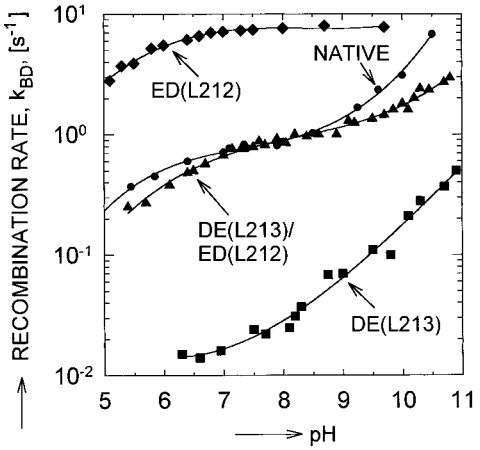

FIGURE 2: The pH dependence of the charge recombination $D^+Q_AQ_B^- \rightarrow DQ_AQ_B$, k_{BD}, monitored *via* the absorbance of the donor at 865 nm as a function of time for native and mutant RCs. The pH was adjusted by adding HCl or NaOH. Native RCs show two pH titrations: one below pH 6 and the other above pH 9. The increase at high pH was shown to be related to the titration of Glu-L212 (*25*, *26*, *31*). The DE(L213) RCs [Glu-L212 → Asp] display decreased values (∼10−15-fold) compared to native RCs over the entire pH range and show only the higher pH titration. Note that the pH at which k_{BD} starts to increase is slightly shifted in the DE-(L213) consistent the creation of a more positive potential near Q_B upon mutation (see text). The smaller k_{BD} values show that Q_B^- is more stable in the DE(L213) mutant RCs than in native RCs at all pH. The ED(L212) RCs [Asp-L213 → Glu] display increased values (∼10-fold) at all pH and show only a lower pH titration. The ED-(L212)/DE(L213) RCs [Glu-L212 → Asp/Asp-L213 → Glu] display similar values (within ∼30%) for k_{BD} as native RCs at all pH, suggesting near-complete electrostatic compensation of Asp-L212 with Glu-L213 (and *vice versa*). The convergence of the rate constants for native and mutant RCs at high pH is expected because k_{BD} can never exceed k_{AD} (∼10 s^{-1}) (*59*) unless the mechanism of charge recombination is changed. Conditions: ∼1−3 μM RCs; 2.5 mM each of Hepes, Caps, Ches, Mes, Pipes, and Tris; 0.04% dodecyl β-D-maltoside; 0.1 mM EDTA, 23 °C.

regions (titrations): one at pH > 9 and the other at pH < 7. The pH profile of k_{BD} in DE(L213) RCs differs from native RCs, with the high pH titration shifted to lower pH by ∼2 pH units. In contrast, only a lower pH titration is observed for k_{BD} in the ED(L212) RCs. The pH profile for k_{BD} measured in the double mutant resembles that observed for native RCs with only minor shifts of the onsets of the high and low pH titrations.

Forward Electron Transfer Rates

Previous studies on RCs with mutations at L212 and L213 showed alterations in either the proton coupled electron transfer rate constant $k_{AB}^{(2)}$ (reaction 1a) or the subsequent protonation event (reaction 1b) (*25*, *26*, *28*−*30*, *50*). The effects of the new mutations on the first and second electron transfer rates were measured by monitoring transient optical absorption changes in native and mutant RCs.

First Electron Transfer $k_{AB}^{(1)}$: $Q_A^-Q_B \rightarrow Q_AQ_B^-$. The electron transfer rate constant $k_{AB}^{(1)}$ was measured in native and mutant RCs (Table 1) by monitoring the absorption change at 750 nm following a saturating laser flash (*59*, *61*). The DE(L213) and ED(L212)/DE(L213) mutant RCs displayed $k_{AB}^{(1)}$ values similar to those of native RCs at pH 7.5 (Table 1). The $k_{AB}^{(1)}$ value for the ED(L212) RCs is ∼20-fold smaller than in native RCs.

Second Electron Transfer $k_{AB}^{(2)}$: $Q_A^-Q_B^- + H^+ \rightarrow Q_AQ_BH^-$. The rate constant $k_{AB}^{(2)}$ was measured by monitoring the decay of the semiquinone absorbance at 450 nm after two laser flashes in the presence of exogenous donors (*62*). The rate constant $k_{AB}^{(2)}$ was reduced ∼9-fold and ∼70-fold in the ED(L212)/DE(L213) and DE(L213) RCs, respectively, compared to native RCs (pH 7.5) (Table 1). In contrast, $k_{AB}^{(2)}$ was increased ∼7-fold in the ED(L212) RCs compared to native RCs.

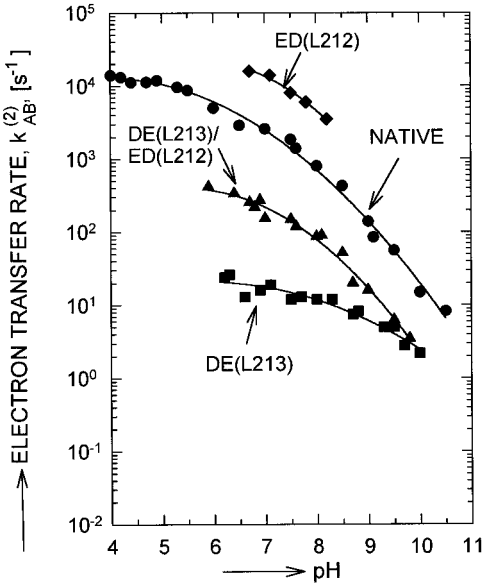

FIGURE 3: The pH dependence of the proton-coupled electron transfer rate constant $k_{AB}^{(2)}$ determined by monitoring the decay of the semiquinone absorbance at 450 nm as a function of time for native and mutant RCs. Note the large decrease (∼10−100-fold) in $k_{AB}^{(2)}$ observed for the DE(L213) RCs over the entire pH range, the decrease (∼10-fold) for ED(L212)/DE(L213) RCs and the increase (∼7-fold) for ED(L212) RCs. The rate constant $k_{AB}^{(2)}$ could only be accurately determined for the ED(L212) RCs over a relatively narrow pH range. Conditions: ∼1−3 μM RCs; 20−500 μM ferrocene or 20 μM cyt *c*; 2.5 mM each of Hepes, Caps, Ches, Mes, Pipes, and Tris; 0.04% dodecyl β-D-maltoside; 0.1 mM EDTA, 23 °C. The pH was adjusted by adding HCl or NaOH.

At higher pH these observations are qualitatively the same, although some quantitative differences were observed (see Figure 3). Native RCs show a rate constant that is approximately proportional to $[H^+]^{0.4}$ at pH ≪ 8 and to $[H^+]^{0.9}$ at pH ≫ 8. The DE(L213) RCs showed a rate constant $k_{AB}^{(2)}$ that was smaller than native values at all pH varying from ∼100-fold smaller at lower pH to ∼10-fold smaller at higher pH. $k_{AB}^{(2)}$ was approximately pH independent below pH ∼8. The pH profile of the double mutant ED(L212)/DE(L213) was very similar to that observed for native RCs, although the $k_{AB}^{(2)}$ values were ∼10-fold smaller than native at all pH. In ED(L212) RCs, the observed rate constant $k_{AB}^{(2)}$ was increased ∼7-fold over the limited pH range where data could be obtained; outside of this pH range either the equilibrium constant *K* (eq 4) became very small (higher pH) or the rate ($k_{AB}^{(2)}$) became too fast to accurately measure with the given experimental setup (lower pH).

The dependence of the rate constant $k_{AB}^{(2)}$ on the redox potential of Q_A^-, *i.e.* the electron driving force, has been previously investigated in native RCs to determine the mechanism of the proton-coupled electron transfer (reaction 1a) (*52*). We used this technique to investigate the mechanism for reaction 1a in the mutant RCs. The native UQ_{10} in the Q_A site was replaced with MQ_4 and TEMNQ, which increase the electron driving force compared to UQ_{10} in native RCs by 46 meV and 120 meV, respectively (*52*). The replacement of UQ_{10} with MQ_4 and TEMNQ in the Q_A site

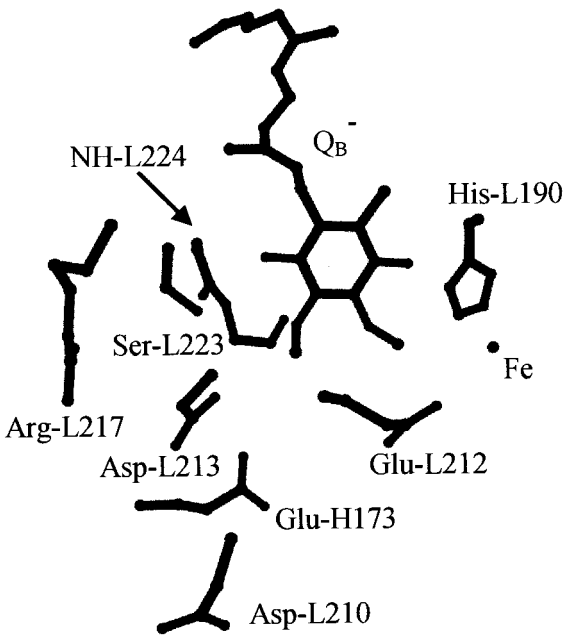

FIGURE 4: Partial RC structure near the secondary quinone, Q_B, binding site, as determined for the Q_B^- state by Stowell *et al.* (*24*) [Brookhaven PDB code 1AIG]. One carbonyl oxygen of Q_B is located near Ser-L223 and the backbone NH of Ile-L224; the other carbonyl oxygen of Q_B is located near His-L190. Nearby are two carboxylic acid groups, Asp-L213 and Glu-L212, that have been implicated in proton transfer to reduced Q_B (reactions 1a and 1b, respectively) (*25*, *26*, *28*−*31*). This structure suggests a possible proton transfer chain from Asp-L213 to Ser-L223 to reduced Q_B. Asp-L213 may acquire its proton from several possible candidates, including Asp-L210, Glu-H173 and/or bound water molecules (not shown).

increased the observed rate constant $k_{AB}^{(2)}$ by ∼4-fold and ∼6.5-fold, respectively, for both native and mutant RCs.

Modeling the Observed pH Profiles of k_{BD}

We have calculated the pH dependences of k_{BD} for native and mutant RCs (data from Figure 2) assuming electrostatic interactions between Q_B^- and several interacting titrating groups using a simplified model for three interacting acids coupled to Q_B^- (see *e.g.* refs 42 and 44). Such a cluster of three acids (L212, H177, and M234) was considered for *Rps. viridis* by Lancaster *et al.* (*45*); they concluded that it was responsible for the bulk of the proton uptake behavior.

In the present analysis, we included the carboxylic acids at L212 and L213 as two of the strongly coupled titrating sites and one other nearby site with similarly strong couplings. Candidates for the third site include Glu-H173 and Asp-L210 (Figure 4) (*24*), which have been shown in previous calculations to have large interactions with the L212 and L213 sites (*42*−*44*). A unique fit to the data was not found; many sets of parameters give adequate fits to the data (data not shown). For example, a good fit of the pH dependence of k_{BD} in native and mutant RCs can be obtained using three titrating amino acids coupled to each other with interaction energies of 3 pK_a units (180 meV). Two of the three acids (modeled as the L212 and L213 carboxylic acids) have a large interaction of 3.5 pK_a units (210 meV) with the semiquinone Q_B^-; one acid has a small interaction of 1 pK_a unit (60 meV) with Q_B^-. A free energy difference of 5.5 pK_a units (330 meV) for the electron transfer from Q_A^- to Q_B was used; this represents the electron driving force when all titrating acids are protonated. Intrinsic pK_a's of 0 for Asp and 3 for Glu at the L212 or L213 site was used for the fits; the third acid was assigned an intrinsic pK_a of 2.5. The intrinsic pK_a's used in these calculations[2] are not the same as those used by Gunner and Honig (*44*), Beroza *et al.* (*42*, *43*), and Lancaster *et al.* (*45*), since many important contribution to the calculated free energies are not explicitly treated, *e.g.* solvation energies or interactions with fixed charges and dipoles. This *ad hoc* simplification to the calculations is a major reason for the low intrinsic pK_a's needed to obtain an adequate fit to the data. It should be noted that this fitting is similar to that performed by Shinkarev and Wraight (*64*) and Shinkarev *et al.* (*65*) with the exception that a third acid is added to the calculation and the nomenclature is different; their use of a pK_a with Q_B^- is equivalent in our nomenclature to the intrinsic pK_a of the acid plus the electrostatic interaction from the two other titrating sites and the semiquinone.

Although many parameter sets gave adequate fits to the data, there were two common features to these parameter sets. First, it was necessary to have a strong electrostatic interaction energy of ∼200 meV (∼3−4 pK_a units) between any pair of titrating sites and between the L212 and L213 sites and Q_B^-. This large electrostatic interaction is not unreasonable given that the titrating sites are in a low dielectric medium inside a protein (see *e.g.* refs 42−45). Second, it was necessary to have an intrinsic pK_a difference of ∼2−3 units of Glu over Asp at both the L212 and L213 sites, much greater than the measured difference seen in solution. The intrinsic pK_a difference of 2−3 units between Asp and Glu is magnified by the strong electrostatic interactions with the other acids leading to the even greater apparent (observed) difference in pK_a of ∼5 units as is seen in the experimental data (Figure 2).

DISCUSSION

The effects of replacing Glu-L212 with Asp and Asp-L213 with Glu in bacterial RCs were investigated by monitoring changes in the photosynthetic growth of mutants and by measuring electron and proton transfer reactions involving Q_B in isolated RCs. Asp and Glu exhibited significant functional differences when located at the same structural position in the RC. The observed functional differences are attributed to a difference in the states of ionization of Asp and Glu (discussed in detail below). In particular, the electrostatic consequence of differing charge states is dramatic for the proton-coupled electron transfer rate constant $k_{AB}^{(2)}$ (reaction 1a). These consequences are discussed within the framework of a two-step model for reaction 1a proposed for native RCs (*52*). The importance of the electrostatic environment for RC function is also discussed.

Differences in the State of Ionization of Asp and Glu at the Same Structural Position

By comparing the charge recombination data for native, DE(L213) and ED(L212) RCs at the same pH (Table 1), it is apparent that the stability of the charge separated state $D^+Q_AQ_B^-$ is affected by the nature of the carboxylic acids present near Q_B. Replacement of Asp-L213 with Glu [DE-

[2] The *apparent* p$K_a$is the experimentally observed inflection point of the fraction of protonated acid as a function of pH. The *intrinsic* pK_a is the pH value at which the fraction of protonated acid is ∼50% assuming no interaction with other titrating sites. For coupled systems, the pH dependence of the protonated fraction of the groups are nonclassical and may exhibit several sigmoidal regions (*i.e.* several apparent pK_a values).

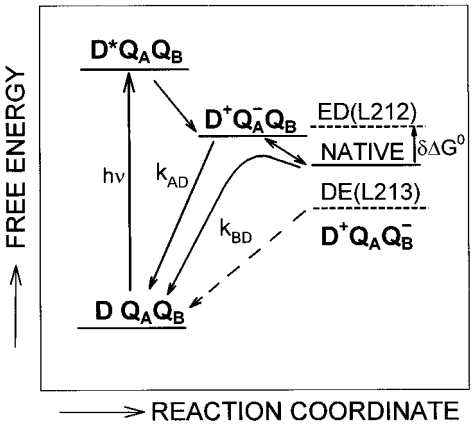

FIGURE 5: Schematic of the charge recombination and the relative energy levels of the relevant states (DQ_AQ_B, $D^*Q_AQ_B$, $D^+Q_A^-Q_B$, and $D^+Q_AQ_B^-$) for native (solid lines) and mutant (dashed) RCs. Recombination from the $D^+Q_AQ_B^-$ state to the ground state in native RCs occurs through a thermal population of the higher energy $D^+Q_A^-Q_B$ state (solid curved line). As the energy level of the final $D^+Q_AQ_B^-$ state is electrostatically raised with respect to the $D^+Q_A^-Q_B$ state, the measured rate of recombination k_{BD} ($D^+Q_AQ_B^- \rightarrow DQ_AQ_B$) is increased as is observed for ED(L212) RCs. The increase in the free energy of the $D^+Q_AQ_B^-$ state, $\delta\Delta G^0$, is indicated. Analogously, as the final $D^+Q_AQ_B^-$ state is lowered with respect to the $D^+Q_A^-Q_B$ state, k_{BD} is decreased as is observed for DE(L213) RCs with recombination occurring directly back to the ground state (dashed lines).

(L213) RCs] decreased the charge recombination rate k_{BD} ($D^+Q_AQ_B^- \rightarrow DQ_AQ_B$) ~15-fold, suggesting a more positive electrostatic potential that stabilizes Q_B^- (see Figure 5). In contrast, replacement of Glu-L212 with Asp [ED(L212) RCs] increased k_{BD} ~10-fold suggesting a more negative electrostatic potential destabilizing Q_B^-. Mutant RCs carrying both replacements showed essentially no change in k_{BD} compared to native RCs, suggesting essentially no change in the electrostatic potential near Q_B.[3] A general trend is apparent which shows that the greater the number of Asp's, the greater the value of k_{BD}. The reverse is also true: the greater the number of Glu's, the smaller k_{BD}. These results suggest that Asp and Glu have different states of ionization with Asp being more ionized (leading to a larger value of k_{BD}) and Glu more protonated (neutral) at either the L212 or L213 site. The pH profiles of k_{BD} suggest that the major points of titration for Asp (*i.e.* the pK_a for a classic titration) is ~6 pH units lower than that of Glu (see Figure 2). This at first sight is surprising in view of the relatively small difference in their pK_a values (0.4 units) in solution (*66*). Several factors may contribute to the large difference in the titration behavior of Asp and Glu at either the L212 or L213 site.

One major contribution to the large apparent pK_a changes arises from large electrostatic interactions with other Asp and Glu sites located nearby in the RC interior (*e.g.* Asp-L210, Glu-H173, see Figure 4). Due to the low dielectric constant in the protein and the small distances between the titrating sites, these interactions are relatively strong. Such strongly interacting titrating sites can show non-classical titration behavior as was calculated by Beroza *et al.* (*42*, *43*) and Gunner and Honig (*44*) for *Rb. sphaeroides* RCs and observed for Glu-L212 in kinetic IR and FTIR studies (*67*, *68*). A simplified model was presented in Paddock *et al.* (*35*) involving two strongly coupled titrating sites. As the pH is increased from below the intrinsic pK_a values of both amino acid groups, the group with the lower intrinsic pK_a (group 1) will titrate first and electrostatically retard the titration of the group with the higher intrinsic pK_a (group 2).[4] This results in an increase in the apparent pK_a for group 2 (see Appendix in ref 35) and has the consequence that if the inherent pK_a of the group 1 is increased (say by an Asp to Glu replacement at L212) above that of group 2, then the apparent pK_a of the group 1 will now be shifted significantly from *its* original value. This provides an explanation for the observed trend that Glu appears to be more protonated than Asp at the same pH; the higher solution pK_a of Glu over that of Asp has been magnified by strong interactions with nearby charged sites leading to a large difference between their states of ionization inside the protein.

Another contribution to the large apparent pK_a differences is a difference in the intrinsic pK_a (see Results). The structural basis for the difference in intrinsic pK_a's could be due to a difference in the solvation of the longer Glu compared to Asp. The solvation energies have been calculated to be large (*i.e.* 3−8 pK_a units; 180−480 meV)[5] within the RC protein (*42*−*45*). Thus, even a relatively small change in the solvation interaction can lead to large changes in the intrinsic pK_a. The differences in solvation arise because these carboxylic acids are located inside the protein where solvation is constrained by the available volume. Large differences in solvation between Asp and Glu at the protein surface would not be expected since water at the surface is not under as many constraints as water in the protein interior. The constraint to internal water molecules is illustrated by the recent crystal structures of the RC which shows many internal ordered water molecules (*21*−*24*). For example, in the native structure of the DQ_AQ_B state, there are three water molecules located within hydrogen bonding distance to Asp-L213 and two waters located near Glu-L212 (*24*). The same thing could happen at the L213 site upon replacing Asp with Glu, *i.e.* reduce the number of nearby water molecules from three to two. This would have the effect of increasing the intrinsic pK_a of Glu over Asp. Another contribution could be due to differences in interaction between Asp and the longer Glu with fixed charges (*e.g.* Arg-L217, see Figure 4) or fixed dipoles from the protein backbone. More sophisticated calculations show that interactions between the titrating site and background interactions in this region can be as large as 7−8 pK_a units (420−480 meV) (*42*−*45*). Thus, a small change in the placement of the titrating site could lead to a change in the intrinsic pK_a similar to that used to fit the data. Conformational changes, caused by the different length of the side chain, could also contribute to the observed difference in the intrinsic pK_a of Glu over that of Asp, although such changes are not required to explain the observed kinetic results presented in this work.

A difference between Asp and Glu at the same structural position has also been observed in bacteriorhodopsin. A large difference in the state of ionization between Asp and

[3] These changes in k_{BD} are attributed solely to alterations in interactions between the protein and the secondary semiquinone Q_B^- and not between the protein and the primary quinone Q_A^-, since k_{AD} remains essentially unchanged in the mutant RCs.

[4] In this senario, the group 1 is either the L212 or L213 residue and the group 2 is some other strongly interacting residue such as Asp-L210 or Glu-H173.

[5] Consider a simple example of solvation energy of a point charge by a fixed dipole of length 1 Å located with its center 3.5 Å from the charge within a low dielectric medium of $\epsilon = 4$ (*e.g.* protein interior). The maximum interaction energy (eq 7) between the charge and the dipole is 300 meV (~5 pK_a units).

Glu at the 85 site was reported by Subramaniam *et al.* (*69*). More recently, Asp-85 was found to titrate with two apparent pK_a's (*70*−*72*) as would be expected for strongly interacting sites. The authors explain this titration behavior by assuming that the titration of the 85 site is coupled to the titration of another internal nearby site (interaction energy of 240 meV, ∼4 pK_a units). This model is similar to that described above. The strong couplings invoked in these models may represent a universal feature of proton transfer systems in proteins.

Interactions between Q_B^- and Carboxylic Acids at the L212 and L213 Sites

Changes in the free energy of the $Q_AQ_B^-$ state with respect to the $Q_A^-Q_B$ state, as shown by the altered k_{BD} values (Table 1), can be quantified using eqs 4 and 5 and the measured charge recombination rate constants k_{AD} and k_{BD} (Table 1). One can define $\delta\Delta G^0$ (Figure 5) to be the observed change in the free energy of the $D^+Q_AQ_B^-$ state of the mutant compared to native RCs. The value of $\delta\Delta G^0$ is ∼−120 meV in the DE(L213) RCs,[6] ∼+100meV in ED(L212) RCs, and ∼0 in the double mutant RCs. These changes in the relative free energy of the $Q_AQ_B^-$ state in the mutant RCs are the result of altered interactions between the charge on Q_B^- and the protein brought about by the amino acid replacement(s). The changes in relative stability result in a corresponding change in the equilibrium constant K, $[Q_AQ_B^-]/[Q_A^-Q_B]$ (see eq 4), from 12 in native RCs to ∼1200 in the DE(L213) and ∼0.2 in the ED(L212). The double mutant ED(L212)/DE(L213) RCs has the same K as native RCs (see Table 1).

Similarly, amino acids near Q_B interact with each other causing pK_a shifts in the mutant RCs which are observed in the pH dependence of k_{BD} (Figure 2). In particular, the onset of the high pH titration, attributed to the titration of Glu-L212 (*25*, *26*, *28*), is shifted to lower pH by ∼2 pH units in the DE(L213) RCs compared to native RCs. The apparent "pK_a" shift of Glu-L212 is a consequence of making the environment of Q_B^- more positive by replacing the ionized Asp with a predominantly neutral Glu at the L213 site. Thus, there is a change in the interaction energy of ∼120 meV (2 pH units) between Glu-L212 and its environment.

To compare our results to previous work (*6*, *7*, *49*, *50*, *64*, *74*), we will make the simplifying assumptions (as has been done before) that the change in the "pK_a" is due to an altered electrostatic interaction between residues at L212, L213, and Q_B^-. If the change in interaction energy is electrostatic, the effective interaction energy between two point charges (q_1, q_2) is given by

$$\delta\Delta G^0 = \frac{q_1 q_2}{4\pi\epsilon_0 r} = \frac{14.4\ \text{eV}}{\epsilon_{\text{eff}} r} \qquad (7)$$

where ϵ_{eff} is the effective dielectric constant and r is the distance in angstroms (Å). For simplicity, we assume that the amino acid replacement results in a charge change of one electronic unit[7] and use for r the distance in the static structure between the carboxylic oxygen of the titrating site-(s) and the center of the quinone head group[8] (*24*, Figure 4). From the values of $\delta\Delta G^0$ (see Table 1), we obtain an effective dielectric ϵ_{eff} between the L212 site and Q_B^- of ∼26, between L213 and the Q_B^- site of ∼22, and between the L212 and L213 sites of ∼16. Thus ϵ_{eff} is in the range of 15−30 in the Q_B binding site; these values are upper limits for the particular interactions, since the change in charge upon mutation may be smaller than unity. Values for ϵ_{eff} in that range were predicted from the observed interaction energy between Asp-L210 and Q_B^- (*74*) and are consistent with the interpretation of proton uptake data (*6*, *7*, *64*, *75*). They are also in good agreement with an empirical distance-dependent expression for the dielectric constant (*76*). Although the results are in agreement with those previously obtained (*6*, *7*, *64*, *75*), it should be noted that interactions between residues have been ignored in the simplified model. This makes it difficult to quantitatively compare the observed interaction energies to calculated interaction energies such as those performed by Beroza *et al.* (*42*, *43*) and Gunner and Honig (*44*); the observed interaction energies are, however, consistent with the large electrostatic interactions predicted by the calculations. Consequently, ϵ_{eff} should be considered as a parameter defined by eq 7 rather than representing the true dielectric constant.

Mechanism of Proton-Coupled Electron Transfer in Native and Mutant RCs

From the observed dependence of $k_{AB}^{(2)}$ on the Q_A^-/Q_A redox potential in native RCs, the mechanism for reaction 1a was proposed to be a two-step process (Figure 6) in which fast reversible proton transfer precedes rate-limiting electron transfer (*51*, *52*). In this work the technique involving Q_A replacement to change the redox potential (*52*) was used to study the mechanism of reaction 1a in mutant RCs. The observed dependence of $k_{AB}^{(2)}$ on the Q_A^-/Q_A redox potential was the same in native and mutant RCs. Thus, the mechanism of reaction 1a is the same in mutant and native RCs, *i.e.* proton transfer remains fast compared to the intrinsic electron transfer ($k_H^+ \gg 10^4\ s^{-1}$) in all mutant RCs (Figure 6).

The observation that the mechanism in the DE(L213) mutant RCs is the same as in native RCs shows that k_{H^+} is large and that the presence of Glu at L213 allows fast proton transfer during reaction 1a. In contrast to the mutant RCs described in this work, it has been previously shown that in the DN(L213) mutant RCs, $k_{AB}^{(2)}$ does not depend on the Q_A^-/Q_A redox potential, consistent with proton transfer being rate limiting for reaction 1a for the DN(L213) mutant RCs (*77*). The change in mechanism when Asn replaces Asp or Glu at L213 supports the proposed role of Asp-L213 in native RCs as a component of a proton transfer chain (*26*, *28*−*30*, *35*, *40*).

Comparison of the Observed $k_{AB}^{(2)}$ with Predictions from the Two-Step Model

Since the results discussed in the previous section show that proton transfer remains fast (compared to electron transfer) in the mutant RCs, how do we explain the difference in the values of the observed $k_{AB}^{(2)}$ in native and mutant RCs?

[6] Since the *direct* rate dominates the observed rate constant k_{BD} for the DE(L213) RCs, we have assumed that the *indirect* component k_{BD}^{ind} is the same ($0.01\ s^{-1}$) as that previously determined for the DN(L213) RCs (*73*). This assumption is based on the similarity of the values and pH profiles for k_{BD} between the DE(L213) and DN(L213) RCs.

[7] The similarity of the values and pH dependences of k_{BD} for DE-(L213) RCs and for DN(L213) RCs (*35*) suggest that Glu-L213 behaves like Asn-L213, *i.e.* Glu is uncharged (protonated).

[8] We assume that the primary effect of the mutations is electrostatic in nature and that conformational changes, if any occur, produce only secondary effects.

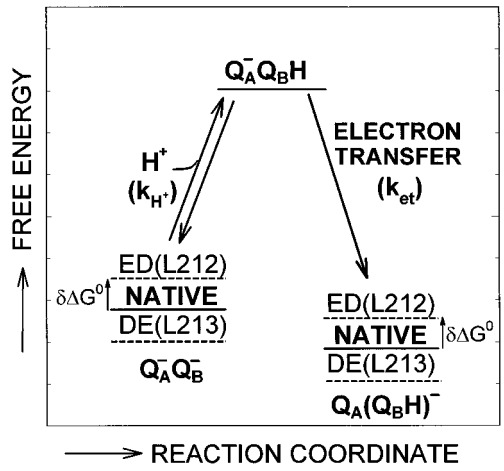

FIGURE 6: Two-step model for the proton-coupled electron transfer (reaction 1a) for native RCs (solid lines) according to Graige *et al.* (*52*). The first step is fast protonation of the semiquinone to establish an equilibration between the initial $Q_A^-Q_B^-$ state and the higher energy intermediate $Q_A^-Q_BH$ state. The second step is rate-limiting electron transfer to form the final $Q_AQ_BH^-$ state. The energy levels of the initial, intermediate, and final states for the DE(L213) and ED(L212) mutant RCs are shown by dashed lines and are labeled for each mutant. Electrostatically the Asp-L213 → Glu replacement [DE(L213)] lowers both the initial and final states without affecting the intermediate state (to first order). As a consequence, the energy gap between the initial and intermediate states is increased resulting in a smaller amount of the intermediate state $Q_A^-Q_BH$ at equilibrium. The energy gap between the intermediate state and the final state will similarly be increased, resulting in a faster intrinsic electron transfer (k_{et}). Since the first step has a greater dependence on the free energy difference (see text), the overall effect is to slow the observed rate. Analogously, the electrostatic effect of the Glu-L212 → Asp [ED(L212)] replacement (to first order) is to raise the energy levels by $\delta\Delta G^0$ (as indicated) of the initial and final states without affecting the intermediate state. By an argument similar to the one presented above, the overall effect is to speed up the observed rate.

Note that there is a correlation between larger values of k_{BD} and larger values of $k_{AB}^{(2)}$ (see Table 1). Since k_{BD} is a measure of the electrostatic environment, this suggests that electrostatics play an important role in determining the effective proton-coupled electron transfer rate (*i.e.* the more negative the electrostatic potential near Q_B, the faster the observed rate). The correlation between k_{BD} and $k_{AB}^{(2)}$ (Table 1) can be rationalized using the two-step model for reaction 1a discussed by Graige *et al.* (*52*) for native RCs. The mechanism involves fast reversible protonation of the semiquinone followed by rate-limiting electron transfer (Figure 6). Thus the observed rate constant $k_{AB}^{(2)}$ is given by

$$k_{AB}^{(2)} = f(Q_BH)k_{et} \tag{8}$$

where $f(Q_BH)$ is the fraction of the protonated intermediate state $Q_A^-Q_BH$ and k_{et} is the microscopic rate constant for the electron transfer step (Figure 6). Changes in the electrostatic environment caused by the mutation change the energetics of proton and electron transfers since these reactions involve transfer of a charged species and therefore should respond to changes in the local electrostatic environment.

The primary effects of the mutations are assumed to be electrostatic and localized at the Q_B site, since the amino acid replacements involve changes of titrating sites located near Q_B. Experimental support for this assumption comes from the unaltered values for k_{AD} and the altered values for k_{BD} measured in the mutant compared to native RCs. Thus, we will explain the observed dependence of $k_{AB}^{(2)}$ on changes in the electrostatic environment caused by mutation by assuming that the mutations affect through electrostatic interactions the relative energies of the initial $Q_A^-Q_B^-$ and final $Q_A(Q_BH)^-$ states (Figure 6). The intermediate state $Q_A^-Q_BH$ is not affected by the electrostatic changes to first order because Q_A^- is far from the site of mutation and Q_BH is electrostatically neutral.

Electrostatic changes near Q_B result in two competing effects on $k_{AB}^{(2)}$. The first effect is a change in the energy gap between the initial ($Q_A^-Q_B^-$) and the intermediate ($Q_A^-Q_BH$) state (Figure 6). This changes the relative equilibrium fraction of the intermediate state by the Boltzmann factor $\exp(+\delta\Delta G^0/kT)$ where $\delta\Delta G^0$ is the change in the initial energy level (see Figure 6), k is Boltzmann's constant, and T is the temperature. Thus, if the potential near Q_B becomes more negative (as is the case for the ED(L212) mutant RCs), *i.e.* $\delta\Delta G^0 > 0$, the energy gap *decreases*, resulting in the formation of a larger fraction of the intermediate state with a concomitant *increase* in $k_{AB}^{(2)}$.

The second effect is a change in the energy gap between the final ($Q_AQ_BH^-$) and the intermediate ($Q_A^-Q_BH$) states. This change in the energy gap has the opposite effect on $k_{AB}^{(2)}$ from the analogous change discussed above. If the potential near Q_B becomes more negative [as is the case for the ED(L212) mutant RC example discussed above], the energy gap *decreases*, reducing the driving force for electron transfer thereby *decreasing* the electron transfer rate according to the Marcus theory (*78*). If the driving force for electron transfer, ΔG_{et}^0, and the change in the energy gap resulting from the mutation, $\delta\Delta G^0$, are small compared to the reorganization energy (*i.e.* $|\Delta G_{et}^0|$, $|\delta\Delta G^0| \ll \lambda$), then the relative change in the electron transfer rate constant is to first order proportional to[9] $\exp(-\delta\Delta G^0/2kT)$, assuming that λ does not change upon amino acid substitution.[10] Because of the factor of 2 in the exponential term, the second step is less sensitive than the first step to changes in the free energy and $k_{AB}^{(2)}$ is, therefore, dominated by the first step, *i.e.* a more negative potential increases $k_{AB}^{(2)}$.

One can derive the quantitative relation for the relative change in $k_{AB}^{(2)}$. Assuming that the energy level of the intermediate state remains unchanged and the change in the initial and final energy levels are identical,

$$\frac{k_{AB}^{(2)\prime}}{k_{AB}^{(2)}} \cong \exp\left\{\frac{\delta\Delta G^0}{2k_BT}\right\} \tag{9}$$

where $k_{AB}^{(2)\prime}$ and $k_{AB}^{(2)}$ are the observed rates in mutant and native RCs, respectively and $\delta\Delta G^0$ is the change in the initial

[9] The assumptions that the reorganization energy λ is larger than the change in free energy $\delta\Delta G^0$ upon mutation (*i.e.* $\lambda \gg |\Delta G_{et}^0|$, $|\delta\Delta G^0|$) and in the electron driving force ΔG_{et}^0 are justified as $\lambda \sim 1.2$eV (*73*) and both $\delta\Delta G^0$ (see Discussion) and ΔG_{et}^0 (*52*) are approximately an order of magnitude smaller.

[10] This simplified form of the Marcus theory (*78*) for the ratio of rate constants in mutant to native RCs comes from the first-order expansion of the activation energy $(\Delta G_{et}^0 + \lambda)^2/4\lambda$ under the assumptions that $\lambda \gg |\Delta G_{et}^0|$, $|\delta\Delta G^0|$. This results in the factor of 2 in the denominator of the exponential.

and final energy levels. We will use the charge recombination data to obtained a value for $\delta\Delta G^0$ (see Table 1). Let us now compare the observed changes in $k_{AB}^{(2)}$ with those predicted by eq 9. The observed consequence of replacing Asp-L213 with Glu [DE(L213) RCs] on the proton-coupled electron transfer rate $k_{AB}^{(2)}$ ($DQ_A^-Q_B^- + H^+ \rightarrow DQ_AQ_BH^-$) was to reduce the observed rate ~70-fold, that of replacing Glu-L212 with Asp [ED(L212) RCs] was to increase $k_{AB}^{(2)}$ ~7-fold, and that of replacing both groups (double mutant) was to reduce $k_{AB}^{(2)}$ ~10-fold compared to native RCs (see Table 1). The predicted changes in $k_{AB}^{(2)}$ using eq 9 are to reduce the observed rate ~11-fold in the DE(L213) RCs, increase $k_{AB}^{(2)}$ ~7-fold in the ED(L212) RCs, and be essentially the same in the double mutant RCs compared to native RCs. Although the quantitative behavior is not accurately predicted for the mutant RCs, the predicted qualitative behavior is indeed observed. A major reason for the quantitative discrepancies is that the relevant potential is at different positions for k_{BD} and $k_{AB}^{(2)}$ (discussed in the next section).

Correlation between $k_{AB}^{(2)}$ and k_{BD}

The origin of the correlation between k_{BD} and $k_{AB}^{(2)}$, mentioned above, is that both rate constants are dependent on the electrostatic environment around Q_B. The charge recombination rate constant k_{BD} depends on the relative energy level of the $Q_AQ_B^-$ state (Figure 5) whereas $k_{AB}^{(2)}$ is dependent on the relative energies of the initial $Q_A^-Q_B^-$, intermediate $Q_AQ_BH^-$ and final $Q_A(Q_BH)^-$ states (Figure 6). Thus both rate constants are sensitive to the energy level of the semiquinone Q_B^- state, *i.e.* to the electrostatic environment.

We have observed an increase in $k_{AB}^{(2)}$ in the ED(L212) RCs (Table 1, Figure 6) as expected from an increase in the energy level of the Q_B^- state as shown by the larger k_{BD} values (Table 1). In contrast, a decrease in $k_{AB}^{(2)}$ is observed in DE(L213) RCs in which the reduced value of k_{BD} shows a lowering of the energy level of the initial Q_B^- state (Figure 5).[11]

Although one sees a general correlation between k_{BD} and $k_{AB}^{(2)}$ as discussed above, the correlation is not expected to be perfect since the relevant potential is at different positions on the quinone ring for the two processes. For k_{BD} the electron is delocalized on the two carbonyl oxygens (~60%) and the rest on the conjugated ring (~40%). Hence, the charge recombination is sensitive to the average potential over the quinone head group and the relevant potential is approximately at the center of the quinone ring. However, for the $k_{AB}^{(2)}$ process (reaction 1a, Figure 6) the relevant electrostatic potential is on the O1 oxygen of the quinone head group (Figure 4) where protonation takes place. These considerations explain the results on the double mutant ED(L212)/DE(L213). In these mutant RCs, the nearby negatively charged amino acid has been moved from Asp-L213 to Asp-L212 (see Figure 4). Because the distance from the carboxylic acid oxygens of these two residues to the center of the quinone ring remains approximately the same, k_{BD} is expected to remain unchanged, as is experimentally observed (see Table 1). However, because the negative charge on Asp-L212 in the double mutant RCs is farther away from the O1 carbonyl oxygen of Q_B than the negative charge on Asp-L213 in the native, $k_{AB}^{(2)}$ is expected to be smaller as is experimentally observed (see Table 1).

From these arguments, it is more justifiable to compare the observed rates between RCs that have a single amino acid change at the L212 site while retaining the same amino acid at the L213 which is closer to the O1 oxygen of the quinone head group. Thus, we will compare ED(L212) to native RCs and ED(L212)/DE(L213) to DE(L213) RCs, to minimize any systematic error made in using the k_{BD} data to determine $\delta\Delta G^0$ for the two-step mechanism (eq 9). Comparing the effects observed in the ED(L212) RCs to those in native we find that $k_{AB}^{(2)}$ is increased (7 ± 2)-fold. Using the data from Table 1 and eq 9 above, an observed increase of 6−9-fold is expected which agrees well with the observed difference. Comparing ED(L212)/DE(L213) to the DE(L213) RCs, an increase of (7 ± 2)-fold is observed and 8−11-fold is predicted, which also agrees well with the observed difference. The agreement of the experimental observations to the predictions from the two-step model (Figure 6) suggest that the effect of the mutations on the observed rate constant is due primarily to the electrostatic changes caused by the amino acid replacement(s) which change the relative energy gaps between the initial, intermediate, and final energy states (Figure 6). In addition, the agreement between experiment and predictions from the model gives additional support for the two-step mechanism. A more detailed discussion of electrostatic changes in site-directed mutant RCs and the effects of these changes on $k_{AB}^{(2)}$ is the subject of a following paper.

Role of Electrostatics in the Function of the Reaction Center

The function of the RC is to mediate an efficient photochemical conversion of quinone to quinol through a set of reactions shown in Figure 1. Changes in the electostatic potential around Q_B brought about by the mutations described in this work drastically effect this conversion by affecting the rate constants $k_{AB}^{(1)}$, $k_{AB}^{(2)}$, and/or the equilibrium constant, K, between the state $Q_AQ_B^-$ and $Q_A^-Q_B$ (eq 5). How do the electrostatic changes affect the quinone/quinol conversion rate and what is the optimal potential around Q_B? To answer these questions, we need to distinguish two cases important for photosynthetic growth: light-limiting and light-saturating conditions.

Light-Limiting Conditions. In this case, the rate of photon absorption per RC is $\ll k_{AB}^{(1)}, k_{AB}^{(2)}$. This implies that an equilibrium between the two states $Q_AQ_B^-$ and $Q_A^-Q_B$ will be established before the RC can absorb another photon. Since RCs in the $Q_A^-Q_B$ state are photochemically inactive, *i.e.* they cannot absorb a second photon, the conversion process will be proportional to the fraction of RCs in the active $Q_AQ_B^-$ state and the photon flux,[12] *i.e.*

[11] In principle, one can have a kinetic barrier due to the introduction of an apparent high pK_a group (pK_a > 7) in a proton transfer pathway as is the case in the DE(L213) RCs. However, proton transfer remains functionally fast and any functional consequences of the *kinetic* barrier introduced by placing Glu at L213 are hidden by the larger consequences of this replacement on the *thermodynamics* of the proton transfers.

[12] We assume that all RCs absorbing a second photon proceed in the photocycle (Figure 1) to the initial state, *i.e.* they are driven to completion by exchange with exogenous quinone.

$$\text{conversion rate} \propto (\text{photon flux})\left(\frac{Q_AQ_B^-}{Q_A^-Q_B + Q_AQ_B^-}\right) = (\text{photon flux})\left(\frac{k_{AB}^{(1)}}{k_{AB}^{(1)} + k_{BA}^{(1)}}\right) \quad (10)$$

In native RCs, $K = 12$ (pH 7.5), *i.e.* 92% of the RCs are in the photochemically active state $Q_AQ_B^-$ after absorption of one photon. In the ED(L212) RCs, the potential near Q_B is more negative raising the energy level of Q_B^- by ~100 meV. This reduces *K* from 12 to 0.2, thereby decreasing the fraction of Q_B^- to 17% and making the conversion rate ~5-fold less effective than in native RCs. Thus, under light-limiting conditions, ED(L212) RCs are much inferior to native RCs. Making the potential more positive cannot improve the fraction of Q_B^- significantly, it being already 92% in native RCs. In addition, as discussed in the next section, the positive potential has a detrimental effect under light-saturating conditions.

Light-Saturating Conditions. In this case, the rate of photon absorption per RC is $\gg k_{AB}^{(1)}$, $k_{AB}^{(2)}$. Under these conditions, equilibrium between the states $Q_AQ_B^-$ and $Q_A^-Q_B$ is not established prior to absorption of a second photon (*i.e.* the back reaction $k_{BA}^{(1)}$ (see Figure 1) has no chance to take place) and, therefore, K is not a relevant parameter for the quinone/quinol conversion rate. Instead, the two important processes acting in series are $Q_A^-Q_B \rightarrow Q_AQ_B^-$ and $Q_AQ_B^- + 2H^+ \rightarrow Q_AQ_BH_2$, which proceed with rate constants $k_{AB}^{(1)}$ and $k_{AB}^{(2)}$, respectively. Since in the first reaction a negative charge (electron) is transferred to Q_B, whereas the rate of the second is mostly determined by transfer of a positive charge (proton), the two reactions are facilitated by electrostatic potentials of the opposite sign. This is illustrated in the ED(L212) RCs in which the increased negative potential near Q_B decreases $k_{AB}^{(1)}$ but increases $k_{AB}^{(2)}$ relative to native RCs (see Table 1). Does this mean that ED(L212) mutant RCs are superior under light-saturating conditions? The answer is no because $k_{AB}^{(1)}$ is now considerably smaller in the mutant and is now the slower step in the photocycle (Figure 1). Thus, under neither set of light conditions is the ED(L212) RCs superior to native RCs.

Why not make the electrostatic potential more positive? The more positive potential has the effect of decreasing $k_{AB}^{(2)}$. This is illustrated by the DE(L213) RCs in which the rate constant $k_{AB}^{(2)}$ is decreased ~70-fold (pH 7.5) compared to native RCs. Thus, although a more positive electrostatic potential can modestly increase the fraction of Q_B^- (as discussed in the previous section), the DE(L213) RCs are inferior to native RCs under light-saturating conditions.

For light-saturating conditions, the potential near Q_B^- for a maximum turnover rate should have a value that makes $k_{AB}^{(1)} = k_{AB}^{(2)}$.[13] For native RCs this is only approximately the case because $k_{AB}^{(1)} = 7k_{AB}^{(2)}$ (pH 7.5) (see Table 1). To make the two rates equal requires a potential near Q_B^- that is ~30 meV more negative than that found in native RCs. However, the trade-off of this electrostaic change would be a reduction in *K* from 12 to 3.3, reducing the fraction of RCs in the photochemically active $Q_AQ_B^-$ state under light-limiting conditions to ~75%.

[13] We neglect for simplicity the possible effects of the change in electrostatic potential or mutation on the quinone/quinol binding constants or exchange rate.

The above considerations suggest that the electrostatic potential near Q_B^- should have a value that provides effective electron and proton-coupled electron transfer ($k_{AB}^{(1)}$ and $k_{AB}^{(2)}$) important under light-saturating conditions as well as a favorable equilibrium of the photochemically active $Q_AQ_B^-$ state that is important for function under light limiting conditions. The potential in native RCs approximately satisfies this criterion.

CONCLUSIONS

The replacement of the seemingly similar Glu for Asp or Asp for Glu led to surprising changes in the characteristics of bacterial RCs. First, the stability of the charge separated state $D^+Q_AQ_B^-$ was dependent on the nature of the carboxylic acids present near Q_B^- and indicated that Asp and Glu have very different state of ionization at either the L212 or L213 structural positions with Asp being more ionized. Second, the change in the electrostatic environment caused by mutation had significant observable effects on the proton coupled electron transfer rate constant $k_{AB}^{(2)}$ [$DQ_A^-Q_B^- + H^+ \rightarrow DQ_A(Q_BH)^-$] which can be explained using the proposed reaction mechanism of fast reversible protonation of the semiquinone followed by rate-limiting electron transfer. Third, the electrostaic potential near Q_B^- is finely tuned to allow both efficient proton transfer as well as efficient electron transfer to the secondary quinone, allowing for efficient growth under both light-limiting and light-saturating conditions.

ACKNOWLEDGMENT

We thank Ed Abresch and Andrea Juth for technical assistance and Michael Graige for many helpful discussions.

REFERENCES

1. Breton, J., and Vermeglio, A., Eds. (1992) *The Photosynthetic Bacterial Reaction Center II: Structure, Spectroscopy and Dynamics*, Plenum Press, New York.
2. Feher, G., Allen, J. P., Okamura, M. Y., and Rees, D. C. (1989) *Nature 339*, 111−116.
3. Crofts, A. R., and Wraight, C. A. (1983) *Biochim. Biophys. Acta 726*, 149−185.
4. Maroti, P., and Wraight, C. A. (1990) in *Current Research in Photosynthesis* (Baltscheffsky, M., Ed.) Vol. 1, pp 1.165−1.168, Kluwer, Boston.
5. Gunner, M. (1991) *Curr. Topics Bioenerg. 16*, 319−367.
6. Maroti, P., and Wraight, C. A. (1988) *Biochim. Biophys. Acta 934*, 329−347.
7. McPherson, P. H., Okamura, M. Y., and Feher, G. (1988) *Biochim. Biophys. Acta 934*, 348−368.
8. McPherson, P. H., Okamura, M. Y., and Feher, G. (1990) *Biochim. Biophys. Acta 1016*, 289−292.
9. Dutton, P. L. (1986) in *Photosynthesis III: Photosynthetic Membranes and Light Harvesting Systems, Encyclopedia of Plant Physiology* (Staehlin, L. A., and Arntzen, C. J., Eds.) Vol. 19, pp 197−237, Springer, New York.
10. Ort, D. R. (1986) in *Photosynthesis III: Photosynthetic Membranes and Light Harvesting Systems, Encyclopedia of Plant Physiology* (Staehlin, L. A., and Arntzen, C. J., Eds.) Vol. 19, pp 143−196, Springer, New York.
11. Deisenhofer, J., Epp, O., Huber, R., and Michel, H. (1985) *Nature 318*, 618−624.
12. Michel, H., Epp, O., and Deisenhofer, J. (1986) *EMBO J. 5*, 2445−2451.
13. Allen, J. P., Feher, G., Yeates, T. O., Komiya, H., and Rees, D. C. (1987) *Proc. Natl. Acad. Sci. U.S.A. 84*, 5730−5734.
14. Allen, J. P., Feher, G., Yeates, T. O., Komiya, H., and Rees, D. C. (1987) *Proc. Natl. Acad. Sci U.S.A. 84*, 6162−6166.
15. Allen, J. P., Feher, G., Yeates, T. O., Komiya, H., and Rees, D. C. (1988) *Proc. Natl. Acad. Sci U.S.A. 85*, 8487−8491.

16. Deisenhofer, J., and Michel, H. (1989) *Biosci. Rep. 9*, 383−419.
17. Arnoux, B., Ducruix, A., Astier, C., Picaud, M., Roth, M., and Reiss-Husson, F. (1990) *Biochimie 72*, 525−530.
18. Chang, C.-H., El-Kabbani, O., Tiede, D., Norris, J., and Schiffer, M. (1991) *Biochemistry 30*, 5352−5360.
19. El-Kabbani, O., Chang, C.-H., Tiede, D., Norris, J., and Schiffer, M. (1991) *Biochemistry 30*, 5361−5369.
20. Chirino, A. J., Lous, E. J., Huber, M., Allen, J. P., Schenck, C. C., Paddock, M. L., Feher, G., and Rees, D. C. (1994) *Biochemistry 33*, 4584−4593.
21. Ermler, U., Fritzsch, G., Buchanan, S. K., and Michel, H. (1994) *Structure 2*, 925−936.
22. Deisenhofer, J., Epp, O., Sinning, I., and Michel, H. (1995) *J. Mol. Biol. 246*, 429−457.
23. Lancaster, C. R. D., Ermler, U., and Michel, H. (1995) in *Anoxygenic Bacteria*, (Blankenship, R. E., Madigan, M. T., and Bauer, C. E., Eds.) pp 503−526, Kluwer Academic Publishers, Dordrecht, The Netherlands.
24. Stowell, M. H. B., McPhillips, T. M., Rees, D. C., Soltis, S. M., Abresch, E., and Feher, G. (1997) *Science 276*, 812−816.
25. Paddock, M. L., Rongey, S. H., Feher, G., and Okamura, M. Y. (1989) *Proc. Natl. Acad. Sci. U.S.A. 86*, 6602−6606.
26. Takahashi, E., and Wraight, C. A. (1990) *Biochim. Biophys. Acta 1020*, 107−111.
27. McPherson, P. H., Schonfeld, M., Paddock, M. L., Okamura, M. Y., and Feher, G. (1994) *Biochemistry 33*, 1181−1193.
28. Takahashi, E., and Wraight, C. A. (1992) *Biochemistry 31*, 855−866.
29. Paddock, M. L., McPherson, P. H., Feher, G., and Okamura, M. Y. (1990) *Proc. Natl. Acad. Sci. U.S.A. 87*, 6803−6807.
30. Takahashi, E., and Wraight, C. A. (1991) *FEBS Lett. 283*, 140−144.
31. Rongey, S. H., Paddock, M. L., Juth, A., McPherson, P. H., Feher, G., and Okamura, M. Y. (1991) *Biophys. J. 59*, 142 (Abstr.).
32. Bylina, E. J., and Wong, R. (1992) in *Research in Photosynthesis* (Murata, N., Ed.) Vol. 1, pp 369−372, Kluwer, The Netherlands.
33. Leibl, W., Sinning, I., Ewald, G., Michel, H., and Breton, J. (1993) *Biochemistry 32*, 1958−1964.
34. Bibikov, S. I., Bloch, D. A., Cherepanov, D. A., Oesterhelt, D., and Semenov, A. Yu. (1994) *FEBS Lett. 341*, 10−14.
35. Paddock, M. L., Rongey, S. H., McPherson, P. H., Juth, A., Feher, G., and Okamura M. Y. (1994) *Biochemistry 33*, 734−745.
36. Paddock, M. L., Rongey, S. H., McPherson, P. H., Feher, G., and Okamura, M. Y. (1991) *Biophys. J. 59*, 142 (abstr.).
37. Okamura, M. Y., and Feher, G. (1992) *Annu. Rev. Biochem. 61*, 861−896.
38. Takahashi, E., and Wraight, C. A. (1994) in *Advances in Molecular and Cell Biology* (Barber, J., Ed.) pp 197−251, JAI Press, Greenwich, CT.
39. Takahashi, E., and Wraight, C. A. (1995) in *Photosynthesis: From Light to Biosphere* (Mathis, P., Ed.) pp 691−694, Kluwer Academic Publishers, Dordrecht, The Netherlands.
40. Rongey, S. H., Juth, A., Paddock, M. L., Feher, G., and Okamura, M. Y. (1995) *Biophys. J. 68*, 247 (Abstr.).
41. Takahashi, E., and Wraight, C. A. (1996) *Proc. Natl. Acad. Sci. U.S.A. 93*, 2640−2645.
42. Beroza, P., Fredkin, D. R., Okamura, M. Y., and Feher, G. (1992) in *The Photosynthetic Reaction Center* (Breton, J., and Vermeglio, A., Eds.) pp 363−374, Plenum Press, New York.
43. Beroza, P., Fredkin, D. R., Okamura, M. Y., and Feher, G. (1995) *Biophys. J. 68*, 2233−2250.
44. Gunner, M. R., and Honig, B. (1992) in *The Photosynthetic Bacterial Reaction Center II* (Breton, J., and Vermeglio, A., Eds.) pp 403−410, Plenum Press, New York.
45. Lancaster, C. R. D., Michel, H., Honig, B., and Gunner, M. R. (1996) *Biophys. J. 70*, 2469−2492.
46. Hanson, D. K., Baciou, L., Tiede, D. M., Nance, S. L., Schiffer, M., and Sebban, P. (1992) *Biochim. Biophys. Acta 1102*, 260−265.
47. Okamura, M. Y., Paddock, M. L., McPherson, P. H., Rongey, S. H., and Feher, G. (1992) in *Research in Photosynthesis* (Murata, N., Ed.) pp 349−356, Kluwer Academic Publishers, Dordrecht, The Netherlands.
48. Hanson, D. K., Tiede, D. M., Nance, S. L., Chang, C. H., and Schiffer, M. (1993) *Proc. Natl. Acad. Sci. U.S.A. 90*, 8929−8933.
49. Maroti, P., Hanson, D. K., Baciou, L., Schiffer, M., and Sebban, P. (1994) *Proc. Natl. Acad. Sci. U.S.A. 91*, 5617−5621.
50. Sebban, P., Maroti, P., Schiffer, M., and Hanson, D. K. (1995) *Biochemistry 34*, 8390−8397.
51. Graige, M. S., Paddock, M. L., Labahn, A., Bruce, J. M., Feher, G., and Okamura, M. Y. (1995) *Biophys. J. 68*, 246 (Abstr.).
52. Graige, M. S., Paddock, M. L., Bruce, J. M., Feher, G., and Okamura, M. Y. (1996) *J. Am. Chem. Soc. 118*, 9005−9016.
53. Paddock, M. L., Feher, G., and Okamura, M. Y. (1996) *Biophys. J. 70*, 11 (abstr.).
54. Nakamaye, K. L., and Eckstein, F. (1986) *Nucleic Acids Res. 24*, 9679−9698.
55. Lin, X., Williams, J. C., Allen, J. P., and Mathis, P. (1994) *Biochemistry 33*, 13517−13523.
56. Simon, R., Proefer, U., and Puhler, A. (1983) *Bio/Technology 1*, 784−791.
57. Rongey, S. H., Paddock, M. L., Feher, G., and Okamura, M. Y. (1993) *Proc. Natl. Acad. Sci. U.S.A. 90*, 1325−1329.
58. Paddock, M. L., Rongey, S. H., Abresch, E. C., Feher, G., and Okamura, M. Y. (1988) *Photosynth. Res. 17*, 75−96.
59. Kleinfeld, D., Okamura, M. Y., and Feher, G. (1984) *Biochim. Biophys. Acta 766*, 126−140.
60. Van Gelder, B. F., and Slater, E. C. (1962) *Biochim. Biophys. Acta 58*, 593−595.
61. Vermeglio, A., and Clayton, R. K. (1977) *Biochim. Biophys. Acta 461*, 159−165.
62. Kleinfeld, D., Okamura, M. Y., and Feher, G. (1985) *Biochim. Biophys. Acta 809*, 291−310.
63. Labahn, A., Bruce, J. M., Okamura, M. Y., and Feher, G. (1995) *Chem. Phys. 197*, 355−366.
64. Shinkarev, V. P., and Wraight, C. A. (1992) in *The Photosynthetic Reaction Center II* (Deisenhofer, J., and Norris, J. R., Eds.) Vol. 1, pp 193−255 Academic Press, San Diego, CA.
65. Shinkarev, V. P., Takahashi, E., and Wraight, C. A. (1992) in *The Photosynthetic Bacterial Reaction Center* (Breton, J., and Vermeglio, A., Eds.) pp 375−387, Plenum Press, New York.
66. Edsall, J. T., and Wyman, J. (1958) *Biophysical Chemistry*, p 699, Academic Press, New York.
67. Hienerwadel, R., Grzybek, S., Fogel, C., Kreutz, W., Okamura, M. Y., Paddock, M. L., Breton, J., Nabedryk, E., and Mantele, W. (1995) *Biochemistry 34*, 2832−2843.
68. Nabedryk, E., Breton, J., Hienerwadel, R., Fogel, C., Mantele, W., Paddock, M. L., and Okamura, M. Y. (1995) *Biochemistry 34*, 14722−14732.
69. Subramaniam, S., Marti, T., and Khorana, H. G. (1990) *Proc. Natl. Acad. Sci. U.S.A. 87*, 1013−1017.
70. Balashov, S. P., Govindjee, R., Imasheva, E. S., Misra, S., Ebrey, T. G., Feng, Y., Crouch, R. K., and Menick, D. R. (1995) *Biochemistry 34*, 8820−8834.
71. Richter, H.-T., Brown, L. S., Needleman, R., and Lanyi, J. K. (1996) *Biochemistry 35*, 4054−4062.
72. Govindjee, R., Misra, S., Balashov, S. P., Ebrey, T. G., Crouch, R. K., and Menick, D. R. (1996) *Biophys. J. 71*, 1011−1023.
73. Labahn, A., Paddock, M. L., McPherson, P. H., Okamura, M. Y., and Feher, G. (1994) *J. Phys. Chem. 98*, 3417−3423.
74. Paddock, M. L., Juth, A., Feher, G., and Okamura, M. Y. (1992) *Biophys. J. 61*, 153 (Abstr.).
75. Miksovska, J., Maroti, P., Tandori, J., Schiffer, M., Hanson, D. K., and Sebban, P. (1996) *Biochemistry 35*, 15411−15417.
76. Warshel, A., Russell, S. T., and Churg, A. K. (1984) *Proc. Natl. Acad. Sci. U.S.A. 81*, 4785−4789.
77. Graige, M. S., Paddock, M. L., Feher, G., and Okamura, M. Y. (1996) *Biophys. J. 70*, 11 (abstr.).
78. Marcus, R. A., and Sutin, N. (1985) *Biochim. Biophys. Acta 811*, 265−322.

BI971192M